

Hyperbolic embedding of brain networks can predict the surgery outcome in temporal lobe epilepsy

Martin Guillemaud^{1*}, Alice Longhena¹, Louis Cousyn^{1,2},
Valerio Frazzini^{1,2}, Bertrand Mathon^{1,3}, Vincent Navarro^{1,2},
Mario Chavez⁴

^{1*}Paris Brain Institute (ICM), CNRS, Inserm, Sorbonne University, Inria-Paris. Pitié Salpêtrière Hospital, Paris, France.

² AP-HP, Department of Neurology, Epilepsy Unit, Center of Reference for Rare Epilepsies, ERN EPICARE, Pitié Salpêtrière Hospital, Paris, France.

³ AP-HP, Department of Neurosurgery, Pitié Salpêtrière Hospital, Paris, France.

⁴CNRS, Pitié Salpêtrière Hospital, Paris, France.

*Corresponding author(s). E-mail(s): martin.guillemaud@gmail.com;

Abstract

Epilepsy surgery, particularly for temporal lobe epilepsy (TLE), remains a vital treatment option for patients with drug-resistant seizures. However, accurately predicting surgical outcomes remains a significant challenge. This study introduces a novel biomarker derived from brain connectivity changes caused by TLE surgery, analyzed using hyperbolic graph embeddings, to predict surgical success. Using structural and diffusion magnetic resonance imaging (MRI) data from 51 patients, we examined differences in structural connectivity networks associated to surgical outcomes. Our approach uniquely leveraged hyperbolic Poincaré disk embeddings of pre- and post-surgery brain networks, successfully distinguishing patients with favorable outcomes from those with poor outcomes. Notably, the method identified regions in the contralateral hemisphere relative to the epileptogenic zone, whose connectivity patterns emerged as a potential biomarker for favorable surgical outcomes. To validate the model, we employed a leave-one-out cross-validation approach, achieving an area under the curve (AUC) of 0.86

and a balanced accuracy of 0.81. These results underscore the predictive capability of our model and its effectiveness in individual outcome forecasting based on structural network changes. Our findings highlight the use of non-Euclidean hyperbolic graph embeddings to analyze brain networks, offering deeper insights into connectivity alterations in epilepsy, and advancing personalized prediction of surgical outcomes in TLE.

Keywords: Epilepsy, brain networks, hyperbolic geometry, surgery outcome prediction

1 Introduction

Epilepsy is one of the most prevalent neurological disorders, affecting approximately 1% of the global population [1]. Temporal lobe epilepsy (TLE) is the most common form of drug-resistant focal epilepsy, often leading to a significant reduction in quality of life due to recurrent and unpredictable seizures [1]. For drug-resistant epilepsies, which comprise about 30% of cases, resective epilepsy surgery has become a widely accepted therapeutic option aiming at removing the epileptogenic regions [2–4]. However, approximately 30% of these patients continue to experience persistent seizures after surgery [3]. One potential explanation is that seizures may originate from abnormal brain regions that were not resected. Emerging evidence suggests that in TLE, structural abnormalities extend beyond the epileptogenic zone, forming a broader network involved in seizure generation [5, 6]. A more comprehensive understanding of brain connectivity changes associated with favorable surgical outcomes could enhance surgical planning and postoperative care [7, 8].

Although some scoring systems correlate with surgical outcomes [9–11], existing models remain insufficient to reliably guide clinicians in predicting surgical success, leaving a gap in personalized treatment strategies [12, 13]. Over recent decades, clinical data have been combined with markers from preoperative magnetic resonance imaging (MRI), scalp electroencephalography (EEG), intracranial EEG (iEEG), or magnetoencephalography (MEG), to develop predictive tools [14–18]. Features from interictal pathological iEEG activity, such as spikes and high-frequency events in the epileptogenic zone, have been used as biomarkers of surgical success [19, 20]. Connectivity patterns of these events, however, provide more accurate outcome predictions [21, 22]. For example, preoperative iEEG analyses show that resecting weakly homogeneous networks in TLE often leads to poor outcomes [23]. Non-invasive studies have demonstrated the predictive utility of spectral power and coherence features from presurgical scalp EEG [24, 25], and MEG-derived cortical networks, with localized epileptic regions correlating with seizure-free outcomes [17]. Structural abnormalities in MRI, including the morphology of temporal structures, also predict surgical success when compared to normative data [26–28]. Functional connectivity from presurgical fMRI has been associated with postoperative seizure freedom [29], with poor outcomes linked to regional network segregation [30]. Combining fMRI and diffusion MRI (dMRI) data further reveals that neural architecture serves as a robust biomarker for surgical outcomes [31].

Several studies have linked presurgical white matter properties to surgical outcomes, including tract density [32] and diffusion abnormalities in white matter bundles from DTI data [33]. Patient-specific white matter features from dMRI are strong biomarkers of postoperative seizure outcomes [34]. Structural networks derived from DTI provide accurate, individualized outcome predictions [16, 35–37]. Surgical outcomes depend not only on presurgical networks but also on how resection affects brain connectivity [36, 38, 39]. Predictive modeling of multivariate iEEG data has enabled seizure propensity predictions by simulating channel resection [40, 41]. Network-based in-silico simulations assess the “ictogenicity” of brain areas and predict outcomes of virtual resections [42–45]. This study leverages MRI and dMRI data to analyze pre- and postoperative structural brain connectivity changes, aiming to identify novel biomarkers for more precise outcome predictions.

In recent years, brain connectivity networks have emerged as a powerful framework for studying a range of neurological diseases, including neurodegenerative disorders [46, 47], schizophrenia [48], and epilepsy [49, 50]. Representing the brain as a network of nodes (e.g., brain regions, sensors, voxels) and edges (connections) offers a comprehensive view of brain architecture, surpassing traditional region-based approaches [51–53]. Rather than identifying a single cortical area responsible for seizures, network-based approaches have highlighted the critical role of widespread altered connectivity beyond the epileptogenic zone [6, 49, 54].

Brain connectivity networks are typically represented as adjacency matrices or edge lists, but their high dimensionality and sparsity complicate statistical analysis (e.g., node classification, clustering, and link prediction) [53]. To simplify analysis, networks are projected into low-dimensional vector spaces while preserving their structural properties. Although Euclidean embeddings are commonly used, they often require high dimensions and fail to capture key features of complex networks like hierarchical structure [55–57].

Hyperbolic graph embedding has gained attention for its effectiveness in representing complex networks. Unlike Euclidean space, where distances grow linearly, hyperbolic space features exponentially expanding distances, making it ideal for capturing hierarchical and scale-free structures common in real-world networks [58]. This allows for lower distortion embeddings that preserve both local and global connectivity structures more effectively than Euclidean projections [59, 60].

Hyperbolic embeddings offer key advantages for studying brain connectivity. Brain networks exhibit a hierarchical structure, with local clusters of tightly connected regions and long-range connections integrating functional modules [53]. Hyperbolic space naturally captures these properties in a lower-dimensional space [61]. Recent studies have shown that hyperbolic embeddings are effective for exploring brain network disruptions in neurological conditions. For example, hyperbolic embedding has been used to investigate brain network alterations linked to cognitive decline in Alzheimer’s disease [62, 63], and autism spectrum disorder [57].

In epilepsy research, hyperbolic mapping of brain networks has shown potential for localizing connectivity disruptions caused by surgery [64], and identifying brain states at high risk of seizures [65]. In this study, we used hyperbolic graph embedding to analyze pre- and post-surgical brain networks in 51 patients who underwent anterior

temporal lobe resection (ATLR) surgery [36]. Connectivity networks were constructed from diffusion and structural MRI data before and after surgery. Embedding these networks into hyperbolic space enabled a direct comparison of connectivity changes linked to surgical outcomes, allowing us to assess whether pre- and post-surgical network differences could serve as biomarkers for favorable outcomes.

Analysis of networks embedded in hyperbolic space allowed us to evaluate how surgical resection affects brain connectivity by identifying both short- and long-range effects around the surgical region. This approach highlighted specific brain regions contributing to surgical outcome differentiation, providing insights into the anatomical and network-level changes linked to surgical success. In addition to comparing network structures, hyperbolic embeddings were used to build a predictive model for surgical outcomes. Our results demonstrate that hyperbolic geometry offers a novel framework for analyzing and predicting brain network alterations in TLE, with potential to improve understanding of surgical effects and patient-specific outcome prediction.

2 Results

2.1 Comparison of pre- and post-surgery brain networks

The impact of surgery on brain connectivity was quantified by comparing the HypDisp score of each node in the pre- and post-surgery networks embedded in the hyperbolic disk [64]. Fig. 1 illustrates the procedure for one patient. Interestingly, the embedding separates nodes corresponding to the left and right hemispheres in an unsupervised manner.

The interpolated HypDisp scores from the two patient groups (good and poor outcomes) were compared pixel-by-pixel using a Student’s t-test to identify regions in the disk (referred to as “Region of Interest” or ROI) with significant differences ($p \leq 0.05$). As shown in Fig. 2, for patients with left hemisphere surgery, the ROI consists of a single component, while for those with right hemisphere surgery, three ROIs are identified. It is worthy of notice that the representation of networks in the Euclidean space (via diffusion maps [66]) did not reveal any discriminating node associated to the surgical outcome. These results suggest that embedding brain networks in the hyperbolic disk effectively characterizes the surgical impact on brain connectivity related to outcome.

As seen in Fig. 1, the interpolated HypDisp values clearly delineate a region in the hyperbolic disk where surgery significantly alters network structure. Notably, the surgical region does not entirely overlap with the regions whose connectivity is associated to the surgical outcome, indicating that surgery, as a perturbation of the connectivity graph, affects both local and global network structures.

2.2 Surgery outcome prediction

To assess the impact of embedding alignment before HypDisp score calculation on surgery outcome prediction, we repeated the leave-one-patient-out procedure multiple times with different control network references. Evaluating the model across various reference networks from the healthy group, we obtained an Area Under the Curve (AUC) of 0.865 ± 0.003 and a balanced accuracy of 0.81 ± 0.02 (mean value \pm SD).

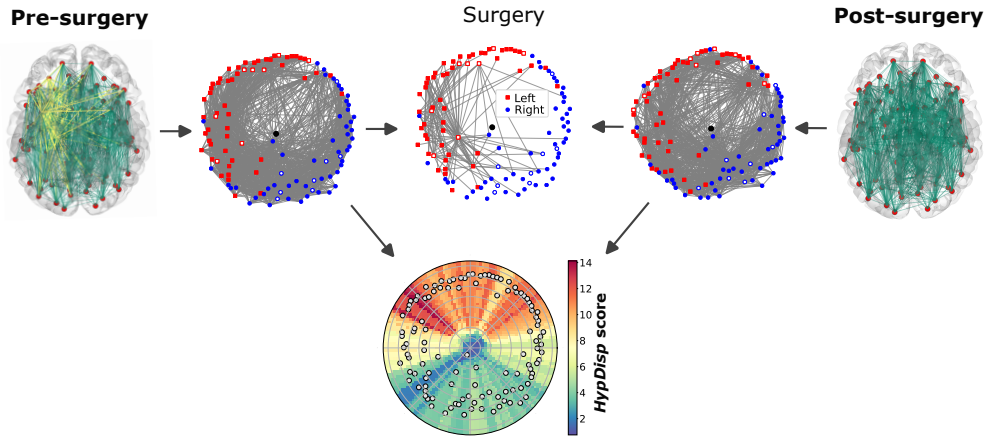


Fig. 1 Embedding and comparison of pre- and post-operative networks in the Poincaré disk. Pre- and post-surgery brain networks are embedded and aligned in the hyperbolic disk. The HypDisp score is calculated for each node and interpolated across the disk for each patient. Red squares represent left hemisphere nodes, blue dots represent right hemisphere nodes, and the black dot marks the origin $(0,0)$ of the Poincaré disk. White-faced nodes correspond to the temporal lobes (left or right, based on edge color). The surgery network represents the connections that were removed during the surgery.

The reduced variability in performance indicates that the choice of reference network had no effect on outcome prediction.

Six patients from the favorable outcome group ($n = 42$) were misclassified as having a poor outcome. Three of these patients relapsed at years 3, 4, and 5, while three others withdrew after three years. Conversely, two patients from the poor outcome group ($n = 9$) were misclassified as favorable outcomes, and both became seizure-free at years 3 and 4. One of these had a marginal probability of 0.51 of being classified as favorable. Prediction analysis for each subgroup yielded an $AUC=0.90 \pm 0.003$ and a balanced accuracy of 0.84 ± 10^{-16} for the 30 patients who underwent left hemisphere surgery, and an AUC of 0.80 ± 0.01 and accuracy of 0.79 ± 0.05 for the 21 patients who underwent right hemisphere surgery.

To assess the impact of connection number on predicted outcomes, we applied our model to surrogate graphs obtained by randomly rewiring the original networks while preserving the degree distribution. For 25% rewiring, the model yielded a mean $AUC=0.59$ and a balanced accuracy of 0.52. As the number of rewired connections increased, the model could no longer distinguish between the two groups (no ROIs identified). These results suggest that the predicted outcome depends on network organization, not just the number of resected connections.

2.3 Brain regions associated to the surgery outcome

To better interpret the nodes in the regions of interest, we back-projected them from the hyperbolic disk into brain space. Fig. 3 shows the nodes in brain space affected by the surgery and those in the discriminant ROIs of the hyperbolic disk. The nodes impacted by the surgery are concentrated in a small region of the operated hemisphere. For clarity, only nodes with $\geq 40\%$ of connections removed are shown. In contrast, the

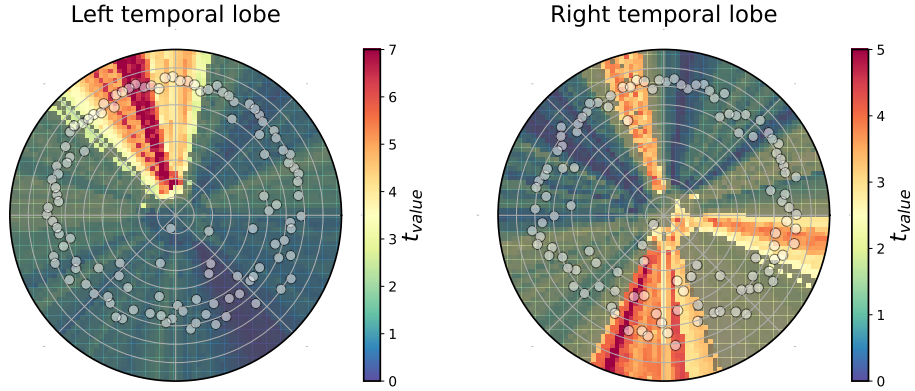


Fig. 2 Pixelwise Student’s t-test comparison of HypDisp score disks between patients with favorable and poor outcomes. Left disk: patients operated on the left temporal lobe; right disk: patients operated on the right temporal lobe. Non-shaded areas represent ROIs with significant differences between the two groups ($p < 0.05$).

nodes differentiating favorable and poor outcomes are mostly located in the contralateral hemisphere, except for one node in the right surgery group. Visual inspection reveals clear hemispherical symmetry between regions impacted by the surgery.

For patients who underwent left hemisphere surgery, the discriminant nodes associated to surgical outcome are concentrated in a small region of the contralateral hemisphere (Fig. 3, bottom plots). In contrast, for those with right hemisphere surgery, the discriminant nodes are more dispersed in the left hemisphere (Fig. 3, top plots). This contralateral localization in both groups highlights the importance of examining the entire patient network, beyond the local regions directly affected by surgery, to accurately assess its impact.

3 Discussion

This study developed a framework to map and characterize the effects of surgery on neuroanatomical connectivity in epileptic patients. We explored embedding brain connectivity networks in non-Euclidean space to predict surgical outcomes in TLE patients. By mapping brain networks onto the Poincaré disk, we identified connectivity changes that may serve as biomarkers for predicting surgical outcomes. Our results suggest that this framework can assess surgical resection impacts and predict outcomes by simulating disconnections in preoperative networks.

In patients with drug-resistant TLE epilepsy, current prognostic models combine clinical, neuroimaging, and electrophysiological data to predict surgical outcomes [10, 12]. However, no method has consistently demonstrated robust predictive power [12, 67]. In this study, we explored embedding brain connectivity networks in hyperbolic space to predict surgical outcomes in TLE patients. Our findings suggest that hyperbolic disk embedding is well-suited for such networks. By mapping pre- and post-surgical networks in this non-Euclidean space, we identified discrepancies that may inform a predictive tool for surgical outcomes. Our approach, which analyzes

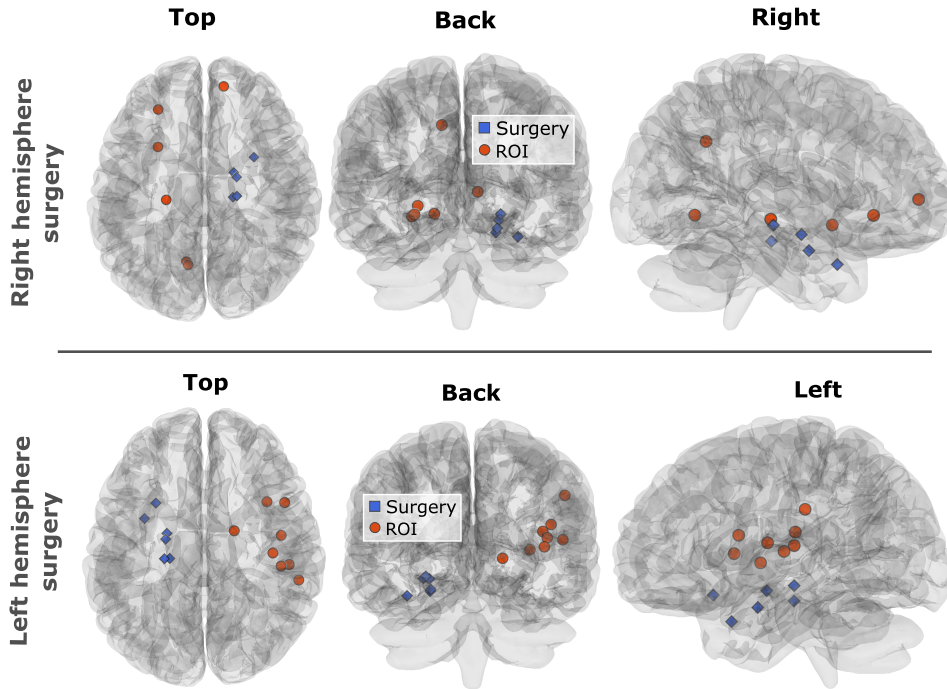


Fig. 3 Projection onto brain space of the regions of interest from the hyperbolic disk showing the greatest outcome differences between groups. The first row shows patients operated on the right hemisphere, and the second row, those operated on the left. Blue points indicate brain areas directly affected by surgery, while red points represent key areas associated with outcome differences, as defined by the ROIs in the Poincaré disk.

brain networks in latent hyperbolic space, offers a novel framework for characterizing and mapping surgery’s effects on neuroanatomical connectivity. We expect these low-dimensional, informative representations to be crucial for brain network studies, surpassing standard network measures and Euclidean embeddings. Notably, no significant differences in the number of connections were found between pre- and post-surgery networks, and Euclidean space representations (via diffusion maps) did not reveal surgical outcome differences.

Recent studies have used brain network data to predict surgical outcomes. Pre-surgical fMRI connectivity networks provided an accuracy of 76% for outcome prediction [68]. Similarly, preoperative brain connectivity from iEEG recordings predicted epilepsy surgery outcomes with 87% accuracy [23]. A connectivity-based simulation model achieved an AUC of 87% [43], while a functional ECoG connectivity model predicted surgery outcomes with 83% accuracy [44]. A dynamical iEEG model predicted surgical outcomes with an AUC of 89% by extracting virtual resection network features [45]. Combining presurgical functional networks (iEEG) with structural connectivity (dMRI) yielded an AUC of = 81% for predicting seizure outcomes [18]. Using structural and functional MRI, connectivity anomalies predicted postsurgical seizure

outcomes with 76% accuracy [29]. Evidence suggests that integrating neuroimaging data (including connectivity) with clinical information can improve predictions, achieving accuracy above 91% [15, 18].

Prediction models based on anatomical connectivity from presurgical DTI data have yielded accuracy values ranging from 70% [69] to 83% [34]. However, these models focus on partial networks, specifically the ipsilateral temporal lobe’s links to extratemporal regions [34]. A deep learning model using presurgical DTI-based connectomes achieved 88% precision [16]. Using high-resolution connectivity reconstructions, a local connectivity group selection predicted surgical outcomes with 95% accuracy, compared to 88% for low-resolution parcellations [70]. Alternatively, quantifying postsurgical connectivity changes predicted seizure outcomes with 79% accuracy [38]. Another study used postsurgery connectivity changes to predict outcomes with an AUC of 84% [18]. Our prediction performances (AUC=86% and balanced accuracy of 81%) are comparable to these studies, though we note that existing accuracy values may be biased toward the majority group of patients with favorable outcomes. In contrast, in our study we accounted for group imbalances by using balanced accuracy.

Our prediction method performed better for patients who underwent left hemisphere surgery (mean AUC=0.90±0.003), identifying a more compact region of interest in the brain. This aligns with studies showing differences between left and right hemisphere surgeries [71, 72]. These differences may be due to larger fiber tracks in left TLE patients compared to right TLE patients and healthy subjects [6, 73]. We identified brain regions potentially involved in surgical failure, aiding in the differentiation of patient groups with distinct outcomes. Notably, the discriminant regions were consistently located in the contralateral hemisphere. While contralateral effects are not widely described, they are observed in TLE. Studies have shown contralateral abnormalities in preoperative DTI [74], positron emission tomography (PET) [75], and interictal scalp EEG data [71]. These abnormalities have also been noted in baseline imaging and electrophysiological data [76]. Brain connectivity studies have found contralateral differences linked to seizure recurrence, with TLE patients showing more connections in the contralateral hemisphere compared to healthy controls [68], along with reduced long-range connections [29, 30]. This reduction in contralateral centrality was also observed in DTI-derived structural networks [35]. Additionally, metabolic network analysis using PET data has linked contralateral connectivity differences to surgical failure [77]. Our findings may reflect postoperative changes, such as contralateral hippocampal atrophy [72], or widespread network reorganization observed in postoperative fMRI connectivity [78].

Our approach has some limitations that future studies should address. First, brain networks here are based on structural connections derived from MRI and dMRI data. However, structural imaging techniques generally assume bi-directional connections, which may inaccurately represent brain connectivity in primates [79]. Additionally, deterministic tractography methods can yield connectivity errors due to the crossing fiber problem [80]. Probabilistic tractography should be preferred for more reliable connectivity networks [81]. To estimate structural connectivity, MRI data is mapped to networks depicting anatomical connections between a reduced number of brain areas,

typically based on an atlas. However, the method of node determination affects network estimates of brain connectivity [82]. Different brain atlases should be evaluated to create networks with more nodes, enhancing spatial resolution [53], and predictive capabilities [70]. Ultimately, Our methodology, based on anatomical brain networks in TLE, can be extended to connectivity networks from other imaging modalities (e.g., fMRI, iEEG) and extra-temporal epilepsies [51, 52, 83]. Furthermore, studying non-invasive connectivity networks (e.g., from EEG and MEG data) could provide a promising presurgical clinical tool.

Our results should be viewed in the context of a limited-size dataset from a previously published study [36]. Postoperative network changes were able to statistically differentiate between favorable and poor outcomes only within the first year after surgery. However, for this limited dataset, creating more refined patient groups, such as those experiencing relapse at three or five years, would have led to more moderate differentiation and prediction. While short-term failure may result from incomplete resection, long-term relapse is influenced by many factors, including changes in medical treatment, lifestyle, and other variables not included in the current database [84]. Incorporating connectivity markers from larger patient groups, along with clinical data, should improve long-term predictions [67].

Computational models informed by brain imaging have provided insights into the networks involved in seizure generation and propagation [43–45]. Using patient-specific structural connectivity from DTI data, network-based simulations have predicted post-surgical outcomes through simulated resections [42]. Our approach offers an alternative to dynamic models for assessing the impact of disconnections and predicting seizure outcomes by performing *in silico* resections. If validated in larger studies, it could improve localization of epileptogenic networks, enhance surgical outcome predictions, and aid in estimating post-injury or post-intervention network reorganization, leading to better follow-up and prognosis.

4 Methods

4.1 Dataset

The dataset includes 51 patients who underwent anterior temporal lobe resection for epilepsy and 29 healthy subjects [36]. Patients are divided into two groups: those who had left (n=30) or right (n=21) temporal lobe surgery. Patients were followed for five years post-surgery and classified according to the International League Against Epilepsy (ILAE) seizure outcome scale at annual intervals [85]. Some patients in the favorable outcome group (seizure-free) experienced relapses at one, two, three, four, or five years [36]. Due to the dataset’s limited size, we focused on the ILAE outcome at one year, resulting in two groups: i) 9 patients (2 males, 7 females) with poor outcomes (ILAE 3-5) who continued to experience seizures, and ii) 34 patients (16 males, 18 females) with favorable outcomes (ILAE 1, seizure-free), plus 8 patients (2 males, 6 females) who had auras but no seizures (ILAE 2). Due to the small sample size, we did not predict outcomes for subgroups at two, three, or five years. For a complete description of the patients’ demographic and clinical data, see Ref. [36].

4.1.1 Brain networks

The brain connectivity networks in this study were derived from anatomical neuroimaging data. Diffusion-weighted magnetic resonance imaging (dMRI) and structural MRI were performed pre-surgery, with only MRI conducted postoperatively. Pre-surgery networks were constructed using pre-surgery MRI and dMRI data. Post-surgery networks were generated by removing the resected brain regions from the pre-surgery dMRI using post-surgery MRI. The connections between brain regions were then identified through the dMRI data, revealing the underlying white matter fiber pathways. Data were discretized using a brain atlas of 114 regions (nodes). Further details on data acquisition and network reconstruction are available in Ref. [36].

4.2 Network’s embedding on the hyperbolic space

Hyperbolic geometry provides a natural framework for embedding complex networks due to its ability to efficiently capture hierarchical and tree-like structures. In the Poincaré disk model, nodes of a graph are mapped to points within a unit disk, where distances grow exponentially as they approach the boundary. The hyperbolic distance $\text{dist}_{hyp}(i, j)$ between each pair of nodes i and j , assigned with radii (r_i, r_j) and angles (θ_i, θ_j) at coordinates (r_i, θ_i) and (r_j, θ_j) in the Poincaré disk, is computed according to the hyperbolic law of cosines [86]:

$$\cosh \text{dist}_{hyp}(i, j) = \cosh r_i \times \cosh r_j - \sinh r_i \times \sinh r_j \times \cos(\pi - |\pi - |\theta_i - \theta_j||) \quad (1)$$

Various techniques (e.g., Mercator [87], HyperMap [88], or Hydra [89], among others) have been developed for projecting graphs into hyperbolic space. These methods typically project the graph onto a hyperboloid, which is then mapped onto a 2D hyperbolic space model like the Poincaré or Klein disk. In this study, we project our networks directly onto the unit hyperbolic Poincaré disk \mathbb{D}^2 using the coalescent embedding method [90], a machine learning-based approach known for its versatility and computational speed [64]. Starting with a binary connectivity graph, this method assigns effective edge weights using a repulsion-attraction rule that prioritizes edges with a significant role in information transmission [90]: $\omega_{ij} = \frac{d_i + d_j + d_i d_j}{1 + CN_{ij}}$, where d_i is the degree of node i and CN_{ij} is the number of common neighbors between node i and j . The resulting network ω_{ij} is then projected onto the two-dimensional disk \mathbb{D}^2 using Isomap [66, 90], a nonlinear dimensional reduction technique. The angular coordinates of the embedded nodes are adjusted uniformly, while maintaining their angular order. Finally, the radius of each node is determined by its rank in descending node degree: $r_i = \frac{2}{\zeta}(\beta \ln i + (1 - \beta) \ln N)$, $i = 1, 2, \dots, N$; where N denotes the number of nodes, ζ a parameter determining space curvature, and β a fading parameter. Here, we used $\zeta = 1$ and $\beta = 0.9$. The radial coordinates are then rescaled to fit them into the unitary disk.

This method maps network’s nodes to points within the disk \mathbb{D}^2 , with radial coordinates reflecting the degree of centrality of each node. Nodes closer to the center are more central, while angular coordinates represent the degree of similarity between

nodes. Nodes with smaller angular distances are more interconnected or similar. This approach combines radial centrality and angular similarity, providing a compact representation of both hierarchical and relational structures in the network.

Before comparing pre- and post-surgery brain connectivities, the embedded networks were realigned to correct for random angular offsets in the nodes' positions within the hyperbolic disk. All networks were aligned with a reference connectivity network from the healthy control group. To assess the effect of the reference network, we performed the outcome prediction using various reference networks from the healthy group.

4.3 Comparison of pre- and post-surgery networks

To compare the brain networks before and after surgery and to elucidate the local impact of the surgical procedure, we employ the HypDisp score, as described in [64]. After aligning the two embeddings, the score assigned to each node is given by its hyperbolic displacement within the disc between the pre- and post-surgery networks. The score $\text{HypDisp}(i)$ attributed to each node i is given by :

$$\text{HypDisp}(i) = \text{dist}_{\text{hyp}}(\text{Pos}_o(i), \text{Pos}_p(i)) \quad (2)$$

where $\text{Pos}_o(i)$ and $\text{Pos}_p(i)$ denote the position on \mathbb{D}^2 of node i from the original and perturbed networks, respectively. $\text{dist}_{\text{hyp}}(a, b)$ is the hyperbolic distance (Eq. 1) between the two points a and b on the disk.

4.3.1 Interpolation of HypDisp scores in \mathbb{D}^2

To compare local perturbations between patient groups, we interpolated the nodes' $\text{HypDisp}(i)$ scores across the entire disk. The space was discretized into pixels, with the number of pixels balancing computation time and node count. Fewer pixels lose information, while a larger number increases computation time without improving precision. We used a regular grid of 80 by 80 pixels for discretization, discarding pixels outside the disk. Although other pixel distributions (e.g., hyperbolic) could be used, we observed no significant impact on the statistical comparisons.

To reduce the computational burden, the value assigned to each pixel j was calculated as the weighted average of the HypDisp scores from its k closest nodes (with the pre-surgery positions) on the disk \mathbb{D}^2 :

$$C(j) = \left(\sum_{i=1}^k \frac{1}{d_{\text{hyp}}(\text{Pos}(j), \text{Pos}_o(i))^\alpha} \right)^{-1} \times \sum_{i=1}^k \frac{1}{d_{\text{hyp}}(\text{Pos}(j), \text{Pos}_o(i))^\alpha} \text{HypDisp}(i) \quad (3)$$

Weights of each neighbor are given by the inverse of their hyperbolic distance to the pixel j with the power α . The more a node is distant from a pixel, the less its

value contributes to the final averaged value. The two parameters k and α do not depend on the data, and were set here to $k = 20$ and $\alpha = 0.1$. One can notice that for low values of α , the interpolation results in a very smoothed map. Conversely, large values of α assigns a greater influence to the closest neighbors of the interpolated pixel, resulting into a map formed by a mosaic of tiles. Similarly, low values of k yield irregularity in the interpolation, whereas an interpolation over a large number of neighbors is highly costly. Through experimentation, the value of $k = 20$ was found to reduce the computational burden without significantly affecting the smoothness of the interpolation.

4.4 Statistical prediction of the surgery outcome

Due to the limited database size, we used a leave-one-out approach to assess our model’s predictive capabilities. This method involves removing one patient, training the model on the remaining patients to identify ROIs in \mathbb{D}^2 , and testing the model on the removed patient. The median of the interpolated hyperbolic scores, HypDisp, for all pixels within the ROIs from the training set was used to apply a logistic regression model and predict the probability of a favorable outcome for each patient. This process was repeated for each patient.

Prediction performance was evaluated using the area under the receiver operating characteristic curve (AUC) and balanced accuracy. Since accuracy can be biased toward the majority class (group of patients with favorable outcomes), we used balanced accuracy, which combines sensitivity and specificity, to account for the dataset imbalance.

Acknowledgements. M.G. acknowledges doctoral support from the Ecole Normale Supérieure de Lyon, France.

Conflict of interest. V. Navarro reports fees from Boards with UCB Pharma, EISAI, Liva Nova, GW Pharma. The remaining authors have no conflicts of interest.

Data availability. The brain networks used in this study are publicly available in the supplementary material of Ref. [36].

Authors contribution. M.G. and M.C.: conceptualization, methodology, investigation, result visualization, and writing-original draft; A.L., L.C. and V.N.: methodology, writing-review and editing; V.F. and B.M.: conceptualization, writing-review and editing

References

- [1] Chan, B. & Lowenstein, D. Epilepsy. *New England Journal of Medicine* **349**, 1257–1266 (2003). URL <https://doi.org/A0.1056/NEJMra0223>.
- [2] Wiebe, S., Blume, W. T., Girvin, J. P. & Eliasziw, M. A randomized, controlled trial of surgery for temporal-lobe epilepsy. *New England Journal of Medicine* **345**, 311–318 (2001). URL <https://doi.org/10.1056/NEJM20010802345050>.

- [3] De Tisi, J. *et al.* The long-term outcome of adult epilepsy surgery, patterns of seizure remission, and relapse: a cohort study. *The Lancet* **378**, 1388–1395 (2011). URL [https://doi.org/10.1016/S0140-6736\(11\)60890-8](https://doi.org/10.1016/S0140-6736(11)60890-8).
- [4] Jobst, B. C. & Cascino, G. D. Resective epilepsy surgery for drug-resistant focal epilepsy: A review. *JAMA* **313**, 285–293 (2015). URL <https://doi.org/10.1001/jama.2014.17426>.
- [5] Bernhardt, B. C., Hong, S., Bernasconi, A. & Bernasconi, N. Imaging structural and functional brain networks in temporal lobe epilepsy. *Frontiers in Human Neuroscience* **7**, 50812 (2013). URL <https://doi.org/10.3389/fnhum.2013.00624>.
- [6] Besson, P. *et al.* Structural connectivity differences in left and right temporal lobe epilepsy. *Neuroimage* **100**, 135–144 (2014). URL <https://doi.org/10.1016/j.neuroimage.2014.04.071>.
- [7] Hsieh, J. K. *et al.* Beyond seizure freedom: Dissecting long-term seizure control after surgical resection for drug-resistant epilepsy. *Epilepsia* **64**, 103–113 (2023). URL <https://doi.org/10.1111/epi.17445>.
- [8] Spencer, S. & Huh, L. Outcomes of epilepsy surgery in adults and children. *The Lancet Neurology* **7**, 525–537 (2008). URL [https://doi.org/10.1016/S1474-4422\(08\)70109-1](https://doi.org/10.1016/S1474-4422(08)70109-1).
- [9] Radhakrishnan, K. *et al.* Predictors of outcome of anterior temporal lobectomy for intractable epilepsy a multivariate study. *Neurology* **51**, 465–471 (1998). URL <https://doi.org/10.1212/WNL.51.2.46>.
- [10] Tonini, C. *et al.* Predictors of epilepsy surgery outcome: a meta-analysis. *Epilepsy Research* **62**, 75–87 (2004). URL <https://doi.org/10.1016/j.eplepsyres.2004.08.006>.
- [11] Garcia Gracia, C. *et al.* Seizure freedom score: A new simple method to predict success of epilepsy surgery. *Epilepsia* **56**, 359–365 (2015). URL <https://doi.org/10.1111/epi.12892>.
- [12] Uijl, S. G. *et al.* Prognosis after temporal lobe epilepsy surgery: the value of combining predictors. *Epilepsia* **49**, 1317–1323 (2008). URL <https://doi.org/10.1111/j.1528-1167.2008.01695.x>.
- [13] Garcia Gracia, C. *et al.* Predicting seizure freedom after epilepsy surgery, a challenge in clinical practice. *Epilepsy & Behavior* **95**, 124–130 (2019). URL <https://doi.org/10.1016/j.yebeh.2019.03.047>.
- [14] Armañanzas, R. *et al.* Machine learning approach for the outcome prediction of temporal lobe epilepsy surgery. *PLoS One* **8**, e62819 (2013). URL <https://doi.org/10.1371/journal.pone.0062819>.

- [15] Memarian, N., Kim, S., Dewar, S., Engel, J. & Staba, R. J. Multimodal data and machine learning for surgery outcome prediction in complicated cases of mesial temporal lobe epilepsy. *Computers in Biology and Medicine* **64**, 67–78 (2015). URL <https://doi.org/10.1016/j.combiomed.2015.06.008>.
- [16] Gleichgerrcht, E. *et al.* Deep learning applied to whole-brain connectome to determine seizure control after epilepsy surgery. *Epilepsia* **59**, 1643–1654 (2018). URL <https://doi.org/10.1111/epi.14528>.
- [17] Aydin, Ü. *et al.* Magnetoencephalography resting state connectivity patterns as indicatives of surgical outcome in epilepsy patients. *Journal of Neural Engineering* **17**, 035007 (2020). URL <http://doi.org/10.1088/1741-2552/ab8113>.
- [18] Sinha, N. *et al.* Intracranial EEG structure-function coupling and seizure outcomes after epilepsy surgery. *Neurology* **101**, e1293 (2023). URL <https://doi.org/10.1212/WNL.0000000000207661>.
- [19] Haegelen, C. *et al.* High-frequency oscillations, extent of surgical resection, and surgical outcome in drug-resistant focal epilepsy. *Epilepsia* **54**, 848–857 (2013). URL <https://doi.org/10.1111/epi.12075>.
- [20] Thomas, J. *et al.* A subpopulation of spikes predicts successful epilepsy surgery outcome. *Annals of Neurology* **93**, 522–535 (2023). URL <https://doi.org/10.1002/ana.26548>.
- [21] González Otárula, K. A., von Ellenrieder, N., Cuello-Oderiz, C., Dubeau, F. & Gotman, J. High-frequency oscillation networks and surgical outcome in adult focal epilepsy. *Annals of Neurology* **85**, 485–494 (2019). URL <https://doi.org/10.1002/ana.25442>.
- [22] Lin, J. *et al.* High frequency oscillation network dynamics predict outcome in non-palliative epilepsy surgery. *Brain Communications* **6**, fcae032 (2024). URL <https://doi.org/10.1093/braincomms/fcae032>.
- [23] Antony, A. R. *et al.* Functional connectivity estimated from intracranial eeg predicts surgical outcome in intractable temporal lobe epilepsy. *PloS one* **8**, e77916 (2013). URL <https://doi.org/10.1371/journal.pone.0077916>.
- [24] Varatharajah, Y. *et al.* Quantitative analysis of visually reviewed normal scalp eeg predicts seizure freedom following anterior temporal lobectomy. *Epilepsia* **63**, 1630–1642 (2022). URL <https://doi.org/10.1111/epi.17257>.
- [25] Sheikh, S. R. *et al.* Machine learning algorithm for predicting seizure control after temporal lobe resection using peri-ictal electroencephalography. *Scientific Reports* **14**, 21771 (2024). URL <https://doi.org/10.1038/s41598-024-72249-7>.

- [26] Feis, D.-L. *et al.* Prediction of post-surgical seizure outcome in left mesial temporal lobe epilepsy. *NeuroImage: Clinical* **2**, 903–911 (2013). URL <https://doi.org/10.1016/j.nicl.2013.06.010>.
- [27] Bernhardt, B. C., Hong, S.-J., Bernasconi, A. & Bernasconi, N. Magnetic resonance imaging pattern learning in temporal lobe epilepsy: classification and prognostics. *Annals of Neurology* **77**, 436–446 (2015). URL <https://doi.org/10.1002/ana.24341>.
- [28] Morita-Sherman, M. *et al.* Incorporation of quantitative mri in a model to predict temporal lobe epilepsy surgery outcome. *Brain communications* **3**, fcab164 (2021). URL <https://doi.org/10.1093/braincomms/fcab164>.
- [29] Larivière, S. *et al.* Functional connectome contractions in temporal lobe epilepsy: Microstructural underpinnings and predictors of surgical outcome. *Epilepsia* **61**, 1221–1233 (2020). URL <https://doi.org/10.1111/epi.16540>.
- [30] DeSalvo, M. N., Tanaka, N., Douw, L., Cole, A. J. & Stufflebeam, S. M. Contralateral preoperative resting-state functional MRI network integration is associated with surgical outcome in temporal lobe epilepsy. *Radiology* **294**, 622–627 (2020). URL <https://doi.org/10.1148/radiol.2020191008>.
- [31] Morgan, V. L. *et al.* Presurgical temporal lobe epilepsy connectome fingerprint for seizure outcome prediction. *Brain Communications* **4**, fcac128 (2022). URL <https://doi.org/10.1093/braincomms/fcac128>.
- [32] Alizadeh, M. *et al.* Hemispheric regional based analysis of diffusion tensor imaging and diffusion tensor tractography in patients with temporal lobe epilepsy and correlation with patient outcomes. *Scientific Reports* **9**, 215 (2019). URL <https://doi.org/10.1038/s41598-018-36818-x>.
- [33] Keller, S. S. *et al.* Preoperative automated fibre quantification predicts postoperative seizure outcome in temporal lobe epilepsy. *Brain* **140**, 68–82 (2017). URL <https://doi.org/10.1093/brain/aww280>.
- [34] Bonilha, L. *et al.* The brain connectome as a personalized biomarker of seizure outcomes after temporal lobectomy. *Neurology* **84**, 1846–1853 (2015). URL <https://doi.org/10.1212/WNL.000000000000154>.
- [35] Gleichgerrcht, E. *et al.* Temporal lobe epilepsy surgical outcomes can be inferred based on structural connectome hubs: a machine learning study. *Annals of Neurology* **88**, 970–983 (2020). URL <https://doi.org/10.1002/ana.25888>.
- [36] Sinha, N. *et al.* Structural brain network abnormalities and the probability of seizure recurrence after epilepsy surgery. *Neurology* **96**, e758 (2021). URL <https://doi.org/10.1212/WNL.0000000000001131>.

- [37] Johnson, G. W., Doss, D. J. & Englot, D. J. Network dysfunction in pre and postsurgical epilepsy: Connectomics as a tool and not a destination. *Current Opinion in Neurology* **35**, 196–201 (2022). URL <https://doi.org/10.1097/WCO.0000000000001008>.
- [38] Taylor, P. N. *et al.* The impact of epilepsy surgery on the structural connectome and its relation to outcome. *NeuroImage: Clinical* **18**, 202–214 (2018). URL <https://doi.org/10.1016/j.nicl.2018.01.028>.
- [39] da Silva, N. M. *et al.* Network reorganisation following anterior temporal lobe resection and relation with post-surgery seizure relapse: A longitudinal study. *NeuroImage: Clinical* **27**, 102320 (2020). URL <https://doi.org/10.1016/j.nicl.2020.102320>.
- [40] Steimer, A., Müller, M. & Schindler, K. Predictive modeling of eeg time series for evaluating surgery targets in epilepsy patients. *Human Brain Mapping* **38**, 2509–2531 (2017). URL <https://doi.org/10.1002/hbm.23537>.
- [41] Müller, M. *et al.* Evaluating resective surgery targets in epilepsy patients: a comparison of quantitative eeg methods. *Journal of Neuroscience Methods* **305**, 54–66 (2018). URL <https://doi.org/10.1016/j.jneumeth.2018.04.021>.
- [42] Hutchings, F. *et al.* Predicting surgery targets in temporal lobe epilepsy through structural connectome based simulations. *PLoS Computational Biology* **11**, e1004642 (2015). URL <https://doi.org/10.1371/journal.pcbi.1004642>.
- [43] Goodfellow, M. *et al.* Estimation of brain network ictogenicity predicts outcome from epilepsy surgery. *Scientific Reports* **6**, 29215 (2016). URL <https://doi.org/10.1038/srep29215>.
- [44] Sinha, N. *et al.* Predicting neurosurgical outcomes in focal epilepsy patients using computational modelling. *Brain* **140**, 319–332 (2017). URL <https://doi.org/10.1093/brain/aww299>.
- [45] Kini, L. G. *et al.* Virtual resection predicts surgical outcome for drug-resistant epilepsy. *Brain* **142**, 3892–3905 (2019). URL <https://doi.org/10.1093/brain/awz303>.
- [46] Seeley, W. W., Crawford, R. K., Zhou, J., Miller, B. L. & Greicius, M. D. Neurodegenerative diseases target large-scale human brain networks. *Neuron* **62**, 42–52 (2009). URL <https://doi.org/10.1016/j.neuron.2009.03.024>.
- [47] Perovnik, M., Rus, T., Schindlbeck, K. A. & Eidelberg, D. Functional brain networks in the evaluation of patients with neurodegenerative disorders. *Nature Reviews Neurology* **19**, 73–90 (2023). URL <https://doi.org/10.1038/s41582-022-00753-3>.

- [48] Van Den Heuvel, M. & Fornito, A. Brain networks in schizophrenia. *Neuropsychology Review* **24**, 32–48 (2014). URL <https://doi.org/10.1007/s11065-014-9248-7>.
- [49] Chiang, S. & Haneef, Z. Graph theory findings in the pathophysiology of temporal lobe epilepsy. *Clinical Neurophysiology* **125**, 1295–1305 (2014). URL <https://doi.org/10.1016/j.clinph.2014.04.004>.
- [50] Gleichgerricht, E., Kocher, M. & Bonilha, L. Connectomics and graph theory analyses: novel insights into network abnormalities in epilepsy. *Epilepsia* **56**, 1660–1668 (2015). URL <https://doi.org/10.1111/epi.13133>.
- [51] Reijneveld, J. C., Ponten, S. C., Berendse, H. W. & Stam, C. J. The application of graph theoretical analysis to complex networks in the brain. *Clinical neurophysiology* **118**, 2317–2331 (2007). URL <https://doi.org/10.1016/j.clinph.2007.08.010>.
- [52] Stam, C. J. Modern network science of neurological disorders. *Nature Reviews Neuroscience* **15**, 683–695 (2014). URL <https://doi.org/10.1038/nrn3801>.
- [53] Fornito, A., Zalesky, A. & Bullmore, E. *Fundamentals of brain network analysis* (Elsevier Academic Press, 2016).
- [54] Richardson, M. P. Large scale brain models of epilepsy: dynamics meets connectomics. *Journal of Neurology, Neurosurgery & Psychiatry* **83**, 1238–1248 (2012). URL <https://doi.org/10.1136/jnmp-2011-301944>.
- [55] Nickel, M. & Kiela, D. Poincaré embeddings for learning hierarchical representations. *Advances in Neural Information Processing Systems* **30** (2017). URL https://proceedings.neurips.cc/paper_files/paper/2017/file/59dfa2df42d9e3d41f5b02bfc32229dd-Paper.pdf.
- [56] Sala, F., Sa, C. D., Gu, A. & Ré, C. Jennifer & Krause, A. D. (eds) *Representation tradeoffs for hyperbolic embeddings*. (eds Jennifer & Krause, A. D.) *Proceedings of the 35th International Conference on Machine Learning*, 4460–4469 (PMLR, 2018). URL <https://proceedings.mlr.press/v80/sala18a.html>.
- [57] Whi, W., Ha, S., Kang, H. & Lee, D. S. Hyperbolic disc embedding of functional human brain connectomes using resting-state fMRI. *Network Neuroscience* **6**, 745–764 (2022). URL https://doi.org/10.1162/netn_a_00243.
- [58] Krioukov, D., Papadopoulos, F., Kitsak, M., Vahdat, A. & Boguñá, M. Hyperbolic geometry of complex networks. *Physical Review E - Statistical, Nonlinear, and Soft Matter Physics* **82**, 036106 (2010). URL <https://doi.org/10.1103/PhysRevE.82.036106>.

- [59] Papadopoulos, F., Kitsak, M., Ángeles Serrano, M., Boguñá, M. & Krioukov, D. Popularity versus similarity in growing networks. *Nature* 2012 489:7417 **489**, 537–540 (2012). URL <https://doi.org/10.1038/nature11459>.
- [60] Boguñá, M., Krioukov, D. & Claffy, K. C. Navigability of complex networks. *Nature Physics* **5**, 74–80 (2008). URL <https://doi.org/10.1038/nphys1130>.
- [61] Allard, A. & Ángeles Serrano, M. Navigable maps of structural brain networks across species. *PLoS Computational Biology* **16**, e1007584 (2020). URL <https://doi.org/10.1371/journal.pcbi.1007584>.
- [62] Baker, C. *et al.* Hyperbolic graph embedding of meg brain networks to study brain alterations in individuals with subjective cognitive decline. *IEEE Journal of Biomedical and Health Informatics* 1–11 (2024). URL <https://doi.org/10.1101/2023.10.23.563643>.
- [63] Longhena, A., Guillemaud, M., De Vico Fallani, F., Migliaccio, R. L. & Chavez, M. Hyperbolic embedding of brain networks detects regions disrupted by neurodegeneration. *arXiv preprint* 2407.16589 (2024). URL <https://doi.org/10.48550/arXiv.2407.16589>.
- [64] Longhena, A., Guillemaud, M. & Chavez, M. Detecting local perturbations of networks in a latent hyperbolic embedding space. *Chaos* **34**, 63117 (2024). URL <https://doi.org/10.1063/5.0199546>.
- [65] Guillemaud, M., Cousyn, L., Navarro, V. & Chavez, M. Hyperbolic embedding of brain networks as a tool for epileptic seizures forecasting. *arXiv preprint* 2406.10184v2 (2024). URL <https://doi.org/10.48550/arXiv.2406.10184>.
- [66] Von Luxburg, U. A tutorial on spectral clustering. *Statistics and computing* **17**, 395–416 (2007). URL <https://doi.org/10.1007/s11222-007-9033-z>.
- [67] Eriksson, M. H. *et al.* Predicting seizure outcome after epilepsy surgery: Do we need more complex models, larger samples, or better data? *Epilepsia* **64**, 2014–2026 (2023). URL <https://doi.org/10.1111/epi.17637>.
- [68] He, X. *et al.* Presurgical thalamic “hubness” predicts surgical outcome in temporal lobe epilepsy. *Neurology* **88**, 2285–2293 (2017). URL <https://doi.org/10.1212/WNL.000000000000403>.
- [69] Munsell, B. C. *et al.* Evaluation of machine learning algorithms for treatment outcome prediction in patients with epilepsy based on structural connectome data. *Neuroimage* **118**, 219–230 (2015). URL <https://doi.org/10.1016/j.neuroimage.2015.06.008>.
- [70] Chen, X., Wang, Y., Kopetzky, S. J., Butz-Ostendorf, M. & Kaiser, M. Connectivity within regions characterizes epilepsy duration and treatment outcome. *Human*

- Brain Mapping* **42**, 3777–3791 (2021). URL <https://doi.org/10.1002/hbm.25464>.
- [71] Pustina, D., Doucet, G., Skidmore, C., Sperling, M. & Tracy, J. Contralateral interictal spikes are related to tapetum damage in left temporal lobe epilepsy. *Epilepsia* **55**, 1406–1414 (2014). URL <https://doi.org/10.1111/epi.12721>.
- [72] Fernandes, D. A. *et al.* Long-term postoperative atrophy of contralateral hippocampus and cognitive function in unilateral refractory MTLE with unilateral hippocampal sclerosis. *Epilepsy & Behavior* **36**, 108–114 (2014). URL <https://doi.org/10.1016/j.yebeh.2014.04.028>.
- [73] Ahmadi, M. E. *et al.* Side matters: diffusion tensor imaging tractography in left and right temporal lobe epilepsy. *American journal of neuroradiology* **30**, 1740–1747 (2009). URL <https://doi.org/10.3174/ajnr.A1650>.
- [74] Concha, L., Beaulieu, C. & Gross, D. W. Bilateral limbic diffusion abnormalities in unilateral temporal lobe epilepsy. *Annals of Neurology* **57**, 188–196 (2005). URL <https://doi.org/10.1002/ana.20334>.
- [75] Cahill, V. *et al.* Metabolic patterns and seizure outcomes following anterior temporal lobectomy. *Annals of Neurology* **85**, 241–250 (2019). URL <https://doi.org/10.1002/ana.25405>.
- [76] Jehi, L. E., Silveira, D. C., Bingaman, W. & Najm, I. Temporal lobe epilepsy surgery failures: predictors of seizure recurrence, yield of reevaluation, and outcome following reoperation. *Journal of Neurosurgery* **113**, 1186–1194 (2010). URL <https://doi.org/10.3171/2010.8.JNS10180>.
- [77] Strýček, O., Říha, P., Kojan, M., Řehák, Z. & Brázdil, M. Metabolic connectivity as a predictor of surgical outcome in mesial temporal lobe epilepsy. *Epilepsia Open* **9**, 187–199 (2024). URL <https://doi.org/10.1002/epi4.12853>.
- [78] Foesleitner, O. *et al.* Language network reorganization before and after temporal lobe epilepsy surgery. *Journal of Neurosurgery* **134**, 1694–1702 (2020). URL <https://doi.org/10.3171/2020.4.JNS193401>.
- [79] Markov, N. T. *et al.* A weighted and directed interareal connectivity matrix for macaque cerebral cortex. *Cerebral Cortex* **24**, 17–36 (2014). URL <https://doi.org/10.1093/cercor/bhs270>.
- [80] Mori, S. & Van Zijl, P. C. Fiber tracking: principles and strategies—a technical review. *NMR in Biomedicine* **15**, 468–480 (2002). URL <https://doi.org/10.1002/nbm.781>.
- [81] Bonilha, L. *et al.* Reproducibility of the structural brain connectome derived from diffusion tensor imaging. *PloS One* **10**, e0135247 (2015). URL <https://doi.org/10.1371/journal.pone.0135247>.

- [82] Zalesky, A. *et al.* Whole-brain anatomical networks: does the choice of nodes matter? *Neuroimage* **50**, 970–983 (2010). URL <https://doi.org/10.1016/j.neuroimage.2009.12.027>.
- [83] Smith, S. M. *et al.* Network modelling methods for fMRI. *Neuroimage* **54**, 875–891 (2011). URL <https://doi.org/10.1016/j.neuroimage.2010.08.063>.
- [84] Bell, G. S. *et al.* Factors affecting seizure outcome after epilepsy surgery: an observational series. *Journal of Neurology, Neurosurgery & Psychiatry* **88**, 933–940 (2017). URL <https://doi.org/10.1136/jnnp-2017-316211>.
- [85] Wieser, H. G. *et al.* ILAE Commission Report. Proposal for a new classification of outcome with respect to epileptic seizures following epilepsy surgery. *Epilepsia* **42** (2001). URL <https://doi.org/10.1046/j.1528-1157.2001.35100.x>.
- [86] Kitsak, M., Voitalov, I. & Krioukov, D. Link prediction with hyperbolic geometry. *Physical Review Research* **2**, 043113 (2020). URL <https://doi.org/10.1103/PhysRevResearch.2.043113>.
- [87] García-Pérez, G., Allard, A., Serrano, M. Á. & Boguñá, M. Mercator: uncovering faithful hyperbolic embeddings of complex networks. *New Journal of Physics* **21**, 123033 (2019). URL <https://doi.org/10.1088/1367-2630/ab57d2>.
- [88] Papadopoulos, F., Psomas, C. & Krioukov, D. Network mapping by replaying hyperbolic growth. *IEEE/ACM Transactions on Networking* **23**, 198–211 (2014). URL <https://doi.org/10.1109/TNET.2013.2294052>.
- [89] Keller-Ressel, M. & Nargang, S. Hydra: a method for strain-minimizing hyperbolic embedding of network-and distance-based data. *Journal of Complex Networks* **8**, cnaa002 (2020). URL <https://doi.org/10.1093/comnet/cnaa002>.
- [90] Muscoloni, A., Thomas, J. M., Ciucci, S., Bianconi, G. & Cannistraci, C. V. Machine learning meets complex networks via coalescent embedding in the hyperbolic space. *Nature Communications* **8**, 1–19 (2017). URL <https://doi.org/10.1038/s41467-017-01825-5>.